


Pair creation, motion, and annihilation of topological defects in two-dimensional nematic liquid crystals

Dario Cortese, Jens Eggers,^{*} and Tanniemola B. Liverpool[†]
School of Mathematics, University of Bristol, Bristol BS8 1TW, United Kingdom

 (Received 4 October 2017; revised manuscript received 16 January 2018; published 20 February 2018)

We present a framework for the study of disclinations in two-dimensional active nematic liquid crystals and topological defects in general. The order tensor formalism is used to calculate exact multiparticle solutions of the linearized static equations inside a planar uniformly aligned state so that the total charge has to vanish. Topological charge conservation then requires that there is always an equal number of $q = 1/2$ and $q = -1/2$ charges. Starting from a set of hydrodynamic equations, we derive a low-dimensional dynamical system for the parameters of the static solutions, which describes the motion of a half-disclination pair or of several pairs. Within this formalism, we model defect production and annihilation, as observed in experiments. Our dynamics also provide an estimate for the critical density at which production and annihilation rates are balanced.

DOI: [10.1103/PhysRevE.97.022704](https://doi.org/10.1103/PhysRevE.97.022704)

I. INTRODUCTION

Topological defects are nontrivial configurations of a spatially varying order parameter that are associated with localized singularities [1]. They are *topological* because these singularities can be classified into distinct groups whose members are related by a *homotopy* [2]. The study of topological defects has a long history: They have been widely studied, for example, in liquid crystals [3,4] optics [5–7], and even more recently in biological tissues [8,9]. In the past few years, there has been a renewed interest from the point of view of topological phase transitions [10,11]. Singularities play a crucial role in determining the structure of many physical problems [12], and it is therefore a tempting idea to describe the dynamics of the system by the motion of its singularities. This program has been followed extensively in describing the motion of vortices in ideal fluid dynamics [13], in the Ginzburg-Landau equation [14], or in Bose-Einstein condensates.

However, many such approaches are based on *dilute* approximations in which the topological defects are (i) both widely separated from each other and (ii) far from the boundaries [3]. The dilute approximation is equivalent to requiring that the deformations induced by each defect to be vanishingly small at the boundaries and in the vicinity of the other defects. If either of these conditions are not satisfied, then these problems become much more challenging as defects can no longer be considered independently of each other or the boundaries.

This is because the field surrounding a single defect core is characterized by a singular phase, which cannot in general be matched to either to the field at the boundaries (at infinity) or the field near the cores of the other singularities. In addition, the topology of the space (defined by the Euler characteristic) in which the vector field (e.g., liquid crystalline order) lives imposes constraints on the number and charges of the

defects via the Poincaré-Hopf theorem [2]. For example, a consistent treatment requires one consider multiparticle states with constraints on the number and charge of the defects, such that the total charge adds up to the Euler characteristic (zero for a flat plane with no holes). Recent experiments on active liquid crystals [15] provide a motivation to address these long-standing issues as under many conditions, activity leads to “chaotic” states with a proliferation of defects [16–20] which, consequently, are not widely separated from each other or boundaries, *requiring* one to go beyond the dilute approximation.

In this paper we characterize and study the dynamics of topological defects in two-dimensional nematic liquid crystals, though we believe the approach we develop to be more generally applicable to other geometric singularities in a variety of physical systems. To be precise, here we will consider only the lowest-energy defects consistent with nematic liquid crystal symmetry, positive and negative half-integer defects or disclinations [3] on a two-dimensional surface. For a plane with no holes, this implies an even number of defects (particles) with equal numbers of positive and negative charges [2]. Although such particle pairs play an important role in many famous physics problems, such as superconductivity (where positive and negative particles form Cooper pairs), or the Kosterlitz-Thouless transition [21] (which results from the disassociation of vortex pairs), multiparticle states are usually not known explicitly.

However, in the present paper we find explicit expressions for many-particle states of singularities in nematic liquid crystals, so-called disclinations [22], which have topological charges of $q = \pm 1/2$. This is particularly exciting since we are thus able to mathematically describe the creation of a defect pair itself, where a pair of oppositely charged particles are formed spontaneously out of a uniform state. Likewise, we characterize the annihilation of pairs of defects, where two particles come together to form a uniform state. We will describe these singular events for an active suspension of elongated particles [16,19] in a nematic liquid crystal phase.

^{*}jens.egg@bristol.ac.uk

[†]t.liverpool@bristol.ac.uk

This is an example of active matter driven out of equilibrium by constituents which consume energy, the study of which has emerged recently as an exciting new field in soft condensed matter [15]. In the experiment, a thin film of microtubules (MT) is suspended on an oil layer. Molecular motors crosslink MT's and induce relative sliding, which induces motion, and pumps energy into the fluid layer.

Without activity, the fluid is at rest, and the system relaxes to a uniformly ordered nematic state, in which all particles are oriented in the same direction. However, activity induces a highly nonuniform state and in particular leads to the creation of a “gas” of defects or disclinations. The random arrangement of defects is due to constant pair-creation and annihilation events. There have been a number of successful large-scale numerical simulations of this system [23–27], based on a standard continuum model of an active fluid [15]. This will serve as a guide for our theoretical calculations.

Previous theoretical attempts at the problem [28–30] were all based on the hypothetical dynamics of a *single* defect [31,32]. This requires ad hoc assumptions on the form of the far field and necessarily introduces a dependence on some length scale, which serves to remove singularities. It is unknown how to identify this length scale uniquely, based on the equations of motion. Our aim here then is therefore to formulate a dynamics for defects based on first principles, relying on the equations of motion only.

II. STATICS: MULTIDEFECT STATES

Let us begin with a description of the equilibrium states of a uniaxial nematic crystal, described by its director, $\mathbf{n} = (\cos \theta, \sin \theta)$, for which the Frank-Oseen free energy is [3]

$$F_{FO} = \frac{K}{2} \int |\nabla \mathbf{n}|^2 d\mathbf{r} = \frac{K}{2} \int |\nabla \theta|^2 d\mathbf{r}. \quad (1)$$

For simplicity, we have used the one-constant approximation $K \equiv K_1 = K_2 = K_3$. It is crucial to note that in a nematic crystal, \mathbf{n} is an axial vector, for which $\mathbf{n} \equiv -\mathbf{n}$. Similarly, the orientation angle θ is defined only up to multiples of π . Points of stationary variation $\delta F_{FO}/\delta \theta = 0$ define (possibly topologically constrained) equilibrium states, which are solutions of Laplace's equation

$$\nabla^2 \theta = 0. \quad (2)$$

However, (2) does not mean that equilibrium states are defined by a simple linear equation; rather, nonlinearities arise because of the equivalence $\theta \equiv \theta \pm \pi$.

It was noted by Oseen [22,33] that (2) admits solutions corresponding to the two-dimensional singularities,

$$\theta_d^{(m/2)}(\mathbf{r}) = \frac{m}{2} \phi, \quad (3)$$

where m is an integer and $\mathbf{r} = r(\cos \phi, \sin \phi)$ is the position vector. The two lowest-order disclinations $m = \pm 1$ are shown in Fig. 1. Half-integer values of the prefactor are allowed in (3), since $\theta = \pm \pi$ is equivalent to $\theta = 0$, so that the director returns to its original state after a full rotation.

Inserting (3) back into (1), one finds the free energy of a single defect to be $F^{(q)} = \pi K q^2 \ln(L/a)$. To make the result finite, we had to introduce a small scale core size a and a large-

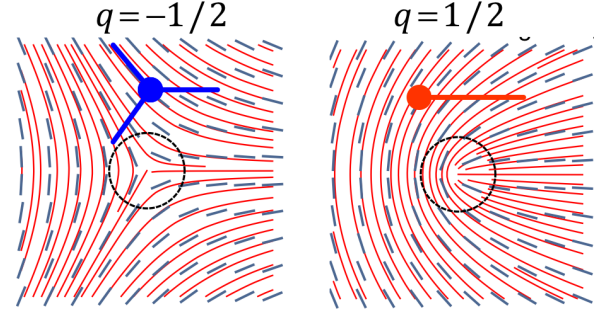


FIG. 1. The disclination (3) for $m = \pm 1$, with charge $q = \pm 1/2$.

scale cutoff L . Both scales will be described self-consistently by the theory we are about to develop. However, it does follow from this simple estimate that in a two-dimensional system the excitations most likely to occur are the two nontrivial lowest-energy states $m = \pm 1$.

The topological character of a defect is defined by its topological charge $q = \frac{1}{2\pi} \oint_C d\theta = \frac{1}{2\pi} \int_0^{2\pi} \frac{d\theta}{d\phi} d\phi$, where C is any closed loop around the defect. Clearly, for the singular solution (3) the result is the charge $q = m/2$, which can take half-integer values. For these half-integer defects, however, there is associated to each defect an attached unbounded singular line at which θ (equivalently \mathbf{n}) jumps $\pm \pi$ (the fact that $\mathbf{n} \equiv -\mathbf{n}$ means that the singular line is an artefact of the parametrization). This highlights the fact that $\mathbf{n}(\mathbf{r})$ is insufficient to describe the singularity completely.

In order to rectify this problem, we use the well-known expression for the nematic free energy, due to de Gennes [3], which includes the additional physics necessary to describe the structure of the core of a defect near its center and removes the artificial singular line. The key is to instead of \mathbf{n} , use as order parameter the symmetric, traceless matrix

$$\mathbf{Q}(\mathbf{r}) = \begin{pmatrix} Q_1 & Q_2 \\ Q_2 & -Q_1 \end{pmatrix} = Q_0 \begin{pmatrix} 2n_x^2 - 1 & 2n_x n_y \\ 2n_x n_y & 1 - 2n_x^2 \end{pmatrix}, \quad (4)$$

thus defining $Q_1(\mathbf{r}), Q_2(\mathbf{r})$, which can also be expressed in terms of the director $\mathbf{n}(\mathbf{r})$ and the degree of alignment $Q_0(\mathbf{r})$ [34]. In particular, the symmetry of \mathbf{n} is now built into the description in that \mathbf{Q} is invariant under the transformation $\mathbf{n} \rightarrow -\mathbf{n}$. In order to guarantee a smooth solution at the core, we use the Landau-de Gennes (LdG) free energy,

$$F_{LdG} = \int \left(-\frac{A}{2} |\mathbf{Q}|^2 + \frac{B}{4} |\mathbf{Q}|^4 + \frac{K}{2} |\nabla \mathbf{Q}|^2 \right) d\mathbf{r}, \quad (5)$$

which allows the amount of nematic ordering to vary. The truncated Landau power series expansion in the invariants of \mathbf{Q} is valid sufficiently close to the isotropic–nematic transition and more and more terms are required as one goes deeper into the nematic phase [35,36]. The transition from the isotropic to the nematic phase occurs in the vicinity of the critical value $A = 0$ (since in general the critical point is modified by fluctuations). The expression above reflects the fact that the isotropic–nematic transition is continuous in two dimensions (it is first order in three dimensions) [3]. In the remainder of this paper we consider the system in the symmetry-broken (nematic) phase where $A > 0$.

Furthermore, we note that there is no way a single defect can be placed in a neutral environment (for example, a constant director $\mathbf{n} = \mathbf{e}_x$) without θ encountering a singularity. The orientation of the constant (uniform) director, reflecting the broken rotational symmetry of the nematic phase, is arbitrary and is chosen here for convenience. Embedding defects into a system with a uniform director requires that the total charge vanishes, which means there must be an equal number of positive and negative half-charges. Thus in any attempt to construct singular solutions which decay to a uniform director field at infinity, one must automatically contemplate many-particle solutions, which incorporate charge neutrality.

At this point it is helpful to be more precise about how we define a defect using the \mathbf{Q} tensor. A defect is localized by the position of the center of its core where there is a phase singularity and $Q_1 = Q_2 = 0$. Its singular nature is indicated by its nonzero charge which can be calculated by the integral of the winding number

$$\begin{aligned} q &= \frac{1}{2\pi} \int_0^{2\pi} \frac{d\theta}{d\phi}(r, \phi) d\phi \\ &= \frac{1}{4\pi} \oint_{C_a} \frac{d}{d\phi} [\arctan(Q_1(r, \phi), Q_2(r, \phi))] d\phi, \end{aligned} \quad (6)$$

calculated on a circle of radius equal to the core size. The value of q allows us to differentiate between different disclinations. Clearly, the integral is unchanged along any closed path $C_{r>a}$ which encompasses the core C_a and contains only one singularity. This invariance of the charge to the variations in the trajectory of the path is why the defects are deemed topological. A path which encloses more than one singularity, e.g., a set of defects with charges $\{q_i\}$, will have a winding number which is the sum of the charges of each of the singularities inside it, $q = \sum_i q_i$. Hence for a system with a uniform director at infinity, this implies a topological constraint of zero total charge, $\sum_i q_i = 0$, e.g., obtained by integrating over a closed circular path with radius $R \rightarrow \infty$ (see Fig. 2).

The elementary disclinations $q = \pm 1/2$ now have the local form,

$$\mathbf{Q}(\mathbf{r}) = Q_0(\mathbf{r}) \begin{pmatrix} \cos \phi & \pm \sin \phi \\ \pm \sin \phi & -\cos \phi \end{pmatrix}, \quad q = \pm \frac{1}{2}. \quad (7)$$

For \mathbf{Q} to be smooth near the origin, $Q_0(r)$ must go to zero for $r \rightarrow 0$, consistent with its interpretation as a measure of local order: At the center of defect, \mathbf{n} points in all directions, so there is no order. As a result, zeros of $Q_0(\mathbf{r}) = \sqrt{Q_1^2(\mathbf{r}) + Q_2^2(\mathbf{r})}$, which are places where $Q_1(\mathbf{r})$ and $Q_2(\mathbf{r})$ vanish simultaneously, are most conveniently used to find the exact position of a disclination. In the following we will embed the defects into an environment with a uniform director field. From a balance of the first two terms of (5), one finds a uniform solution (so that the gradient term disappears) of the form $Q_1 = \bar{Q}_0 \cos \xi$, $Q_2 = \bar{Q}_0 \sin \xi$, where ξ is the (constant) orientation angle and $Q_0 = \sqrt{2A/B}$.

Once more, constrained equilibrium states (with defects located at specified points) are found from the vanishing variation of free energy, $\mathbf{H} = -\delta F_{\text{LDG}}/\delta \mathbf{Q}$, which leads to the pair of nonlinear equations

$$\mathbf{H} = 0 \Rightarrow K \nabla^2 Q_{1,2} + [A - 2B(Q_1^2 + Q_2^2)] Q_{1,2} = 0, \quad (8)$$

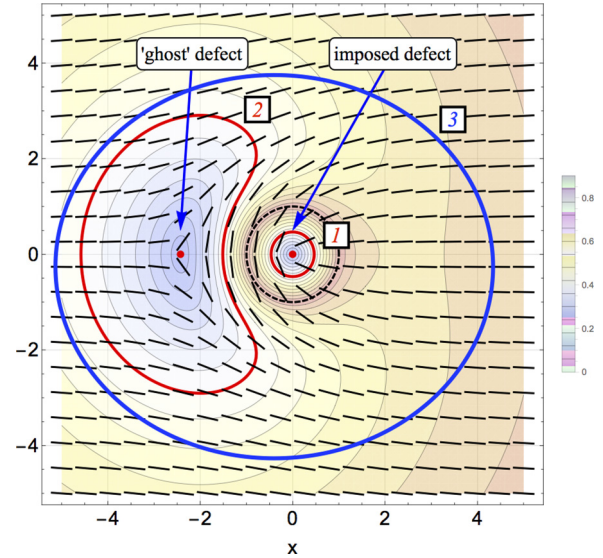


FIG. 2. Director configuration (black bars) and order tensor magnitude (contours) for a pair of oppositely charged half-disclinations. The positive defect on the right was imposed for the solution of equation (9), the negative “ghost” on the left emerges to satisfy the constraint of zero charge. The parameters in Eqs. (13) and (14) are $D_1 = 0.95$, $D_2 = -0.95$; all other parameters are zero. The winding number of the imposed defect on the right obtained by integrating along the loop 1 gives $q_1 = 1/2$ while the winding number of the ghost defect on the left integrating over loop 2 gives $q_2 = -1/2$. The winding number integral over the large loop 3 encompassing both defects is $q = q_1 + q_2 = 0$.

where the constraints are imposed by the boundary conditions on the outer surface of the core of the defect. It makes explicit all the nonlinearities contained implicitly in the invariance property of solutions of (2) and contains additional physics to describe disclinations using smoothly varying fields Q_1, Q_2 . This variation is taking place on a scale of the elastic length $\ell_Q = \sqrt{K/(2A)}$, which follows from a balance of the first and last terms of the free energy (5). The elastic length is much larger than the core radius of the defect a , which is a microscopic scale, set by the size of a molecule. Accordingly, a is the lower limit of physically relevant length scales, below which the continuum model in terms of $\mathbf{Q}(\mathbf{r})$ breaks down. We are interested in solving (8) such that solutions locally describe a $q = \pm 1/2$ disclination yet have a uniform orientation far from the disclination; without loss of generality we take $\xi = 0$, i.e., the nematic is oriented along the x axis.

We linearize (8) around the uniform state, which is given by $\bar{Q}_1 = \bar{Q}_0 = \sqrt{2A/B}$ and $\bar{Q}_2 = 0$: $Q_1 = \bar{Q}_1 + \delta Q_1$, $Q_2 = \delta Q_2$. Thus the linear equations become

$$\nabla^2 \delta Q_1 - \kappa^2 \delta Q_1 = 0, \quad \nabla^2 \delta Q_2 = 0, \quad (9)$$

where $\kappa = \ell_Q^{-1}$. Thus the elastic length scale ℓ_Q sets the size of a defect. In the liquid crystal literature this is also sometimes referred to as the core length scale [34]. We emphasize that this is not the same as the size of the defect core, a which here is a truly *microscopic* length scale where a continuum theory of the type studied in this paper is no longer valid. Denoting the dimensionless inverse elastic length by $\Lambda = \kappa a$, we are interested in the regime for which Λ is small. Linearization

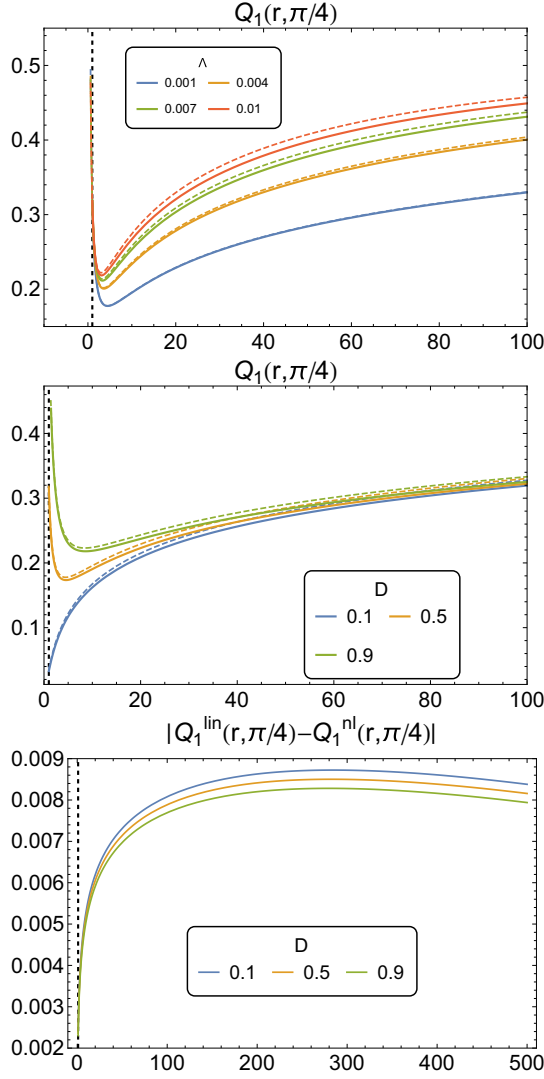


FIG. 3. Comparison between the director configuration from a numerical solution of the nonlinear equation (8) and an analytic solution of the linear approximation (9) for different parameters D, Λ . Distances are measured in units of a . The boundary of the defect core at $r = 1$ is indicated by a vertical line. (a) Linear solution (dashed lines) and nonlinear solutions (solid lines) for $Q_1(r, \phi)$ for different values of Λ . (b) Linear solution (dashed lines) and nonlinear solutions (solid lines) for $Q_1(r, \phi)$ for different $D_1 = D_2 = D$ (parameters of the boundary conditions at $r = 1$ given in (10)). (c) The difference between the linear solution and nonlinear solutions for $Q_1(r, \phi)$ for different $D_1 = D_2 = D$; all other parameters are held fixed, $\zeta_1 = \zeta_2 = \pi/4$.

of the \mathbf{Q} equation makes this problem analytically tractable by assuming variations in Q_0 are small *but* retains all the nonlinearities associated with the variation of the director \mathbf{n} , in that the nonlinear constraint $\mathbf{n} \equiv -\mathbf{n}$ is included. This is a key advantage over (2), typically used to describe defect configurations, which assumes Q_0 to be constant; the price we have paid for this is having to solve two equations instead of one.

In Fig. 3, we show that our linearized solutions agree very well with numerical solutions of the *full* nonlinear equations (8) in the relevant parameter range, both for $r \approx a$ and r large.

In fact, the difference between exact solutions and the linear approximation, shown in part (c) of Fig. 3, demonstrates that the approximation works particularly well near the core $r = a$. This demonstrates that our linearized description (9) contains all the relevant nonlinear topological information implicit in the Q -tensor representation. This is not surprising as this is encoded in the gradient terms which are incorporated *exactly* without any approximations.

Comparison with full numerical solutions of (8) have shown that (9) represents a good approximation to the nonlinear problem. In comparison with (2) (which is equivalent to assuming Q_0 constant), it still contains the nonlinearities which encode the condition $\mathbf{n} \equiv -\mathbf{n}$; the price we have to pay for this is having to solve two equations instead of a single one. Once the solution is found in terms of Q_1, Q_2 , the orientation can be reconstructed by inverting the relations $Q_1 = Q_0 \cos 2\theta$, $Q_2 = Q_0 \sin 2\theta$ to find the orientation angle $\theta(\mathbf{r})$.

Now we solve (9) with boundary condition prescribed at the smallest possible distance a from the origin, chosen so as to impose a phase singularity; by construction, $\delta Q_{1,2}$ have to vanish at infinity, giving the other required boundary condition. The order (topological characteristic) of the phase singularity is specified on the microscopic scale a , much smaller than the physical scale over which fields are varying. This ensures that the macroscopic behavior is not affected by the manner in which the singularity is implemented. The most general ansatz is the Fourier series in ϕ , $Q_\alpha(a, \phi)$:

$$Q_\alpha(a, \phi) = \bar{E}_\alpha + \sum_{n=1}^{\infty} [\bar{D}_\alpha^{(n)} \cos(n\phi + \zeta_\alpha^{(n)})], \quad (10)$$

where $\alpha = \{1, 2\}$. It is here that the topological charge of the *imposed defect* is fixed by the lowest nonzero mode n of (10).

A solution to (9) for $\delta Q_\alpha(r, \phi)$, $\alpha \in \{1, 2\}$ is a superposition of Fourier modes of the form [37]

$$\delta Q_\alpha = \sum_n h_{\alpha,n}(r) (A \cos n\phi + B \sin n\phi). \quad (11)$$

Then $h_{1,n}(r)$ are solutions of a modified Bessel equation [38]; solutions which decay at infinity are

$$K_n(\kappa r) = \int_0^\infty dt \cosh(nt) e^{-\kappa r \cosh t}.$$

This describes the solution for $r > a$, which is the only part of physical interest. The function $h_{2,n}(r) \sim r^{p(n)}$ is a power-law solution of the Laplace equation, with $p > 0$ for $r < a$ and $p < 0$ for $r > a$. We note that while our analysis does allow us to calculate the solutions for $Q_{1,2}(\mathbf{r})$ inside the core ($r < a$), they have no physical significance as the continuum theory is not valid there.

We demonstrate below that only the constant and $n = 1$ terms of the Fourier series for the boundary conditions (10) are required to obtain half-integer disclinations and that the free parameters in (10) and (11) determine the number, locations and orientations of the defects. Hence restricting our analysis first to only the constant (zero mode) and the $n = 1$ mode (easily generalized to higher modes), we require

$$\begin{aligned} Q_1(a, \phi) &= \bar{E}_1 + \bar{D}_1 \cos(\phi + \zeta_1), \\ Q_2(a, \phi) &= \bar{E}_2 + \bar{D}_2 \sin(\phi + \zeta_2), \end{aligned}$$

on $r = a$. The contribution \bar{E}_2 ($n = 0$ term for Q_2) provides a technical difficulty that indicates the topological nature of the problem.

The Laplace equation for δQ_2 only admits power-law solutions which decay to zero as $r \rightarrow \infty$, while a constant solution cannot satisfy both the conditions at the core $\delta Q_2(r = 1) = \bar{E}_2$ and $\delta Q_2 \rightarrow 0$ as $r \rightarrow \infty$. Hence even if the boundary conditions at the core have only 2 terms ($n = 0, 1$), the Fourier series solution for δQ_2 *cannot* be obtained from a finite number of terms. Instead, it can only be achieved by using an infinite number of terms of the series. This illustrates that this solution has global (topological) properties which cannot be captured by local approximations (finite number of Fourier terms). To obtain the solution, we note that rotational invariance implies that the $n = 0$ mode must be constant only in a domain, $\phi \in [-\pi, \pi]$ of size 2π . We can represent it as a sum of Fourier modes, noting the series for a square pulse between $\phi = -\pi$ and $\phi = \pi$ is

$$\bar{E}_2 = \frac{4\bar{E}_2}{\pi} \sum_{n=0}^{\infty} \frac{(-1)^n}{2n+1} \cos \frac{(2n+1)\phi}{2}. \quad (12)$$

Thus the $n = 0$ mode contribution to $\delta Q_2(\mathbf{r})$ can be written as a sum of powers $(a/r)^{n+1/2}$, whose coefficients are the terms in the sum (12) which now satisfies the boundary conditions *both* at $r = 1$ and as $r \rightarrow \infty$.

The resulting expression can be resummed, and if we rescale δQ_1 and δQ_2 with Q_0 , and write r in units of a (such that $r = 1$ at the microscopic size of the defect), we obtain

$$\delta Q_1 = (E_1 - 1) \frac{K_0(\Lambda r)}{K_0(\Lambda)} + D_1 \frac{K_1(\Lambda r)}{K_1(\Lambda)} \cos(\phi + \zeta_1), \quad (13)$$

$$\delta Q_2 = D_2 \frac{\sin(\phi + \zeta_2)}{r} + E_2 f_2(r, \phi), \quad (14)$$

where

$$f_2(x, \phi) = \frac{2}{\pi} \left[\operatorname{arccot} \left(\frac{\sqrt{x}}{\cos \phi/2} + \tan \frac{\phi}{2} \right) + \operatorname{arccot} \left(\frac{\sqrt{x}}{\cos \phi/2} - \tan \frac{\phi}{2} \right) \right].$$

Thus we have obtained for the first time an explicit analytic closed form expression for a disclination pair embedded in a uniformly aligned nematic. Getting a tractable, compact expression for a defect-pair configuration is a significant achievement as this can act as the basis for studies of many defect states.

A couple of examples of typical director configuration are shown in Fig. 4; apart from the imposed $q = 1/2$ defect, a second ‘‘ghost’’ defect has appeared, whose position and orientation depends on the parameters chosen. Thus the total charge of the system is zero, and the director field is uniform far away from the pair. Any solution of Eq. (9) which satisfies uniform boundary conditions must automatically satisfy charge neutrality, to be consistent with the topological nature of the problem.

We can thus characterize a pair of defects in terms of six scalar parameters $D_{1,2}, E_{1,2}$, and $\zeta_{1,2}$. Two examples are illustrated in Fig. 4. Choosing $D > 0$ or $D < 0$, corresponds

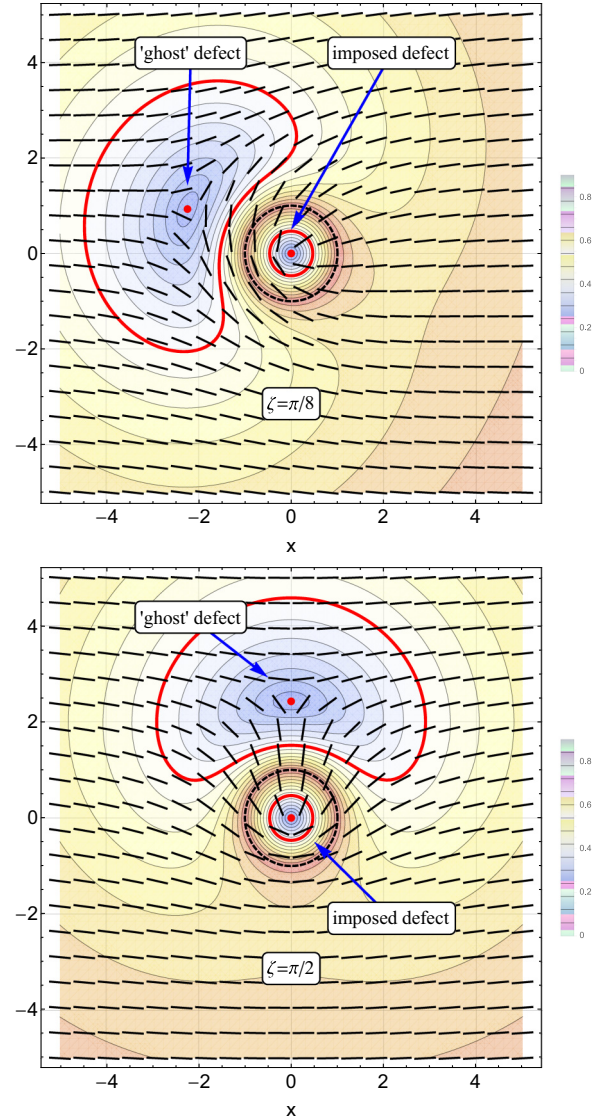


FIG. 4. Director configuration (black bars) and order tensor magnitude (contours) for a pair of oppositely charged half-disclinations. The positive defect was imposed in the solution of Eq. (9), the negative ‘‘ghost’’ emerges to satisfy the constraint of zero charge. Shown are two typical two-defect configurations, as described by (13) and (14), with $D_{1,2} = 0.9, E_{1,2} = 0, \zeta_{1,2} = \pi/8, \pi/4$.

to charge $q = 1/2$ or $q = -1/2$ for the imposed defect, respectively, and thus effectively interchange the imposed and ghost defects. The angles $\zeta_{1,2}$ control the orientation of the imposed defect relative to the order in the far field. The coefficients E_1 and E_2 can be written as $E_1 = E_0 \cos \xi$ and $E_2 = E_0 \sin \xi$, where E_0 controls mainly the degree of anisotropy, whereas ξ is the angle between the two orientations. E_1 and D are the dominant parameters controlling the distance between defects. The distance between the defects is found from solving the simultaneous equations $Q_1 = Q_2 = 0$ for the x, y coordinates of the ghost. This has to be done numerically, and the distance may depend on all parameters. However, E_1 and D are the dominant parameters controlling this.

The six parameters explore the space of static solutions subject to the constraint that a defect be present (without

any constraint, the only equilibrium solution would be a uniform state). We have thus by construction built in the topological constraint of zero total charge, satisfied by all static solutions. Following the model of analytical mechanics, we now study the defect dynamics, which takes place within a reduced space, consistent with a constraint. Our strategy will be to obtain a reduced model in terms of equations of motion for the parameters and then to use the time-dependent parameter values to calculate the time-dependent vortex configurations once the parameter values have been obtained. Equations (13) and (14) correspond to states with at most two defects. However, by including more modes, states with arbitrary number of defects can be generated (see Appendix). Finally, we note that we are also able to obtain explicit solutions for the variation of $\mathbf{Q}(\mathbf{r})$ inside the cores (see Appendix) though these, as mentioned above, are of limited physical relevance because this core scale is comparable to the size of the individual nematogens where our continuum theory is not valid.

III. DEFECT DYNAMICS: PAIR CREATION AND ANNIHILATION

We study the temporal dynamics of disclinations using the standard equations of nematodynamics at vanishing Reynolds number in two dimensions augmented to include the possibility of additional active stresses [15,23]. A key component of nematodynamics are the Stokes equations describing the motion of a viscous nematic fluid [15,23]. They are driven by the active stress $\sigma_a = \alpha c_0^2 \mathbf{Q}$, where c_0 is the concentration of active particles, and the elastic stress, which results from the nematic not being at elastic equilibrium, $\mathbf{H} \neq \mathbf{0}$, as described by (8). A nonvanishing \mathbf{H} indicates an unbalanced elastic stress, so $\sigma_{el} = -\lambda \mathcal{Q}_0 \mathbf{H} + \mathbf{Q} \mathbf{H} - \mathbf{H} \mathbf{Q}$. If $\alpha < 0$ (“pushers”), then the active particles are extensile. The case $\alpha > 0$ (“pullers”) corresponds to contractile particles. The so-called alignment parameter λ will be discussed below. Both extensile and contractile cases lead generically to instability with increasing α , depending on the parameter, λ . Thus Stokes’ equation for an active incompressible nematic fluid $\nabla \cdot \mathbf{v} = 0$ becomes

$$\eta \nabla^2 \mathbf{v} + \nabla \cdot [\sigma_{el} + \sigma_a] = 0. \quad (15)$$

To close the system of equations, we need the equation of motion for \mathbf{Q} :

$$\frac{D\mathbf{Q}}{Dt} = \frac{\mathbf{H}}{\gamma} + \lambda \mathcal{Q}_0 \mathbf{V} - \alpha c_0 (\nabla \cdot \mathbf{Q}) \cdot \nabla \mathbf{Q}, \quad (16)$$

where $V_{ij} = (\partial_i v_j + \partial_j v_i)/2$ and $\omega_{ij} = (\partial_i v_j - \partial_j v_i)/2$ are the symmetric and antisymmetric parts of the velocity gradient tensor $\nabla \mathbf{v}$, respectively. The corotational derivative $D\mathbf{Q}/Dt = \partial_t \mathbf{Q} + \mathbf{v} \cdot \nabla \mathbf{Q} + \boldsymbol{\omega} \mathbf{Q} - \mathbf{Q} \boldsymbol{\omega}$ accounts for the fact that rodlike particles move and rotate with the fluid. The first term on the right of Eq. (4) describes the tendency of the nematic crystal to relax to an elastic equilibrium state, for which $\mathbf{H} = 0$; this occurs on a time scale γ . The next term describes the motion of an elongated particle in shear flow; the dimensionless parameter λ measures the tendency of the particle to align with the flow [39]. A value of $\lambda = 1$ implies total alignment, i.e., particles pointing in the direction of streamlines. Finally, the last term on the right of Eq. (16) accounts for the tendency

of the activity to misalign the nematic, driving it away from equilibrium.

We project the dynamics of \mathbf{Q} , as described by (15) and (16), onto the space of constrained static solutions found in the previous section. Taking into account all Fourier modes would result in an exact representation. To illustrate the approach with a tractable example, we consider the six-dimensional space of solutions contained in (13) and (14), corresponding to restricting our analysis to the first two modes only. In a first step, we linearize the equations in \mathbf{v} , $\delta \mathcal{Q}_1$, and $\delta \mathcal{Q}_2$ to obtain

$$\eta (\nabla^2)^2 \psi = -2[(\alpha + \lambda \Lambda^2) + \lambda \nabla^2] \partial_x \partial_y \delta \mathcal{Q}_1 - \alpha [\partial_x^2 - \partial_y^2] \delta \mathcal{Q}_2 + [(1 - \lambda) \partial_x^2 + (1 + \lambda) \partial_y^2] \nabla^2 \delta \mathcal{Q}_2, \quad (17)$$

$$\partial_t \delta \mathcal{Q}_1 = \lambda (\partial_x \partial_y \psi) + \nabla^2 \delta \mathcal{Q}_1 - \Lambda^2 \delta \mathcal{Q}_1, \quad (18)$$

$$\partial_t \delta \mathcal{Q}_2 = 2[(\lambda + 1) \partial_y^2 \psi + (1 - \lambda) \partial_x^2 \psi] + \nabla^2 \delta \mathcal{Q}_2, \quad (19)$$

writing the velocity in terms of the stream function ψ [40] as $\mathbf{v} = (\partial_y \psi, -\partial_x \psi)$.

We expand in the small parameters λ and α , since for $\lambda = \alpha = 0$ the equations of motion reduce to the equilibrium case, with no motion. At each order $\lambda^n \alpha^m$ in an expansion in the two variables, we can derive an equation of motion for the coefficients of the equilibrium solutions. First, we expand each of the coefficients into a Taylor series in λ, α , which results in a corresponding series for $\delta \mathcal{Q}_{1,2}$: $\delta \mathcal{Q}_{1,2} = \lambda \delta \mathcal{Q}_{1,2}^{(\lambda)} + \alpha \delta \mathcal{Q}_{1,2}^{(\alpha)} + \dots$; and the stream function ψ can be expanded in the same way. As boundary conditions we impose that $\psi^{(\lambda)}$ vanishes at infinity and satisfies the no-slip condition $\psi^{(\lambda)} = \partial_r \psi^{(\lambda)} = 0$ on $r = 1$ [41], corresponding to the microscopic defect core. This condition fixes a frame of reference in which the imposed defect is at rest. We perform the expansion to order λ^2 and $\lambda \alpha$ yielding equations of motion for the parameters, $E_{1,2}(t), D_{1,2}(t), \zeta_{1,2}(t)$,

$$\dot{E}_1(t) = (\bar{\lambda}^2 + \alpha \bar{\lambda}) \frac{1 - E_1^{(0)}}{4\eta}, \quad \dot{E}_2 = 0, \quad (20)$$

$$\dot{D}_1(t) = -\frac{D_1^{(0)}}{4\eta} [\alpha \bar{\lambda} - \bar{\lambda}^2 \sec(2\zeta_1^{(0)})], \quad (21)$$

$$\dot{\zeta}_1(t) = \frac{\bar{\lambda}^2}{4\eta} \tan(2\zeta_1^{(0)}), \quad (22)$$

$$\dot{D}_2(t) = \frac{D_1^{(0)}}{4\eta} [-2\bar{\lambda} \cos(\zeta_1^{(0)} + \zeta_2^{(0)}) + \alpha \sec 2\zeta_2^{(0)} \sin(\zeta_1^{(0)} - \zeta_2^{(0)})], \quad (23)$$

$$\dot{\zeta}_2(t) = \frac{D_1^{(0)}}{2\eta} \frac{D_2^{(0)}}{D_2^{(0)}} [\bar{\lambda} \sin(\zeta_1^{(0)} + \zeta_2^{(0)}) - \alpha \sec 2\zeta_2^{(0)} \cos(\zeta_1^{(0)} - \zeta_2^{(0)})], \quad (24)$$

whose time evolution determines the motion of defects to be described below. We have introduced $\bar{\lambda} = \Lambda \lambda = \kappa a \lambda$ as the rescaled inverse length scale emerging from the interplay of alignment and nematic elasticity. With this rescaling, all explicit dependence on the microscopic cut-off parameter a has dropped out, as it should: the dynamics should not depend

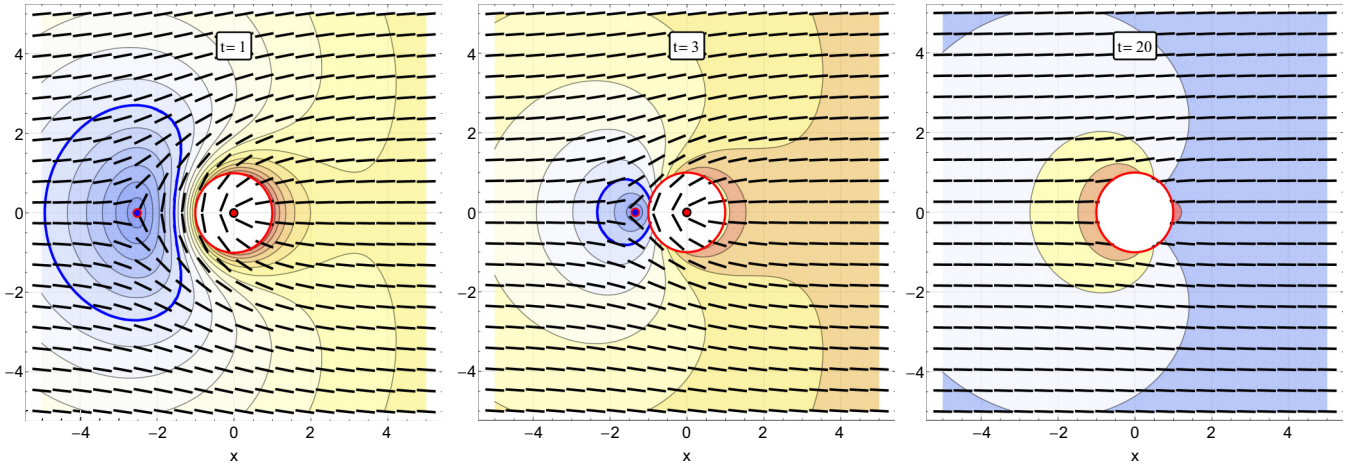


FIG. 5. Dynamics of a passive nematic, $\alpha = 0$. The three panels show the director and degree of order for $\lambda = 0.1$, during the gradual annihilation of the two defects, that relax onto a state with uniform director $\mathbf{n} = \mathbf{e}_x$. $\mathbf{I}(D_1, D_2 E_1, E_2, \zeta_1, \zeta_2)^{(0)} = (0.05, 0.05, -0.5, 0.1, 0, 0)$ and $\Lambda = 10^{-3}$.

on our choice of microscopic cutoff. To find the trajectory of defects, one needs to find the position of their cores by finding the regions where nematic order vanishes by solving for $Q_1 = Q_2 = 0$ at each time step. Since our microscopic scale is a , a pair of defects whose centers have a separation less than a is equivalent to a composite defect whose charge is the sum of the individual topological charges. For equal and opposite charge defects this corresponds to pair annihilation.

A. Passive dynamics

We begin by describing the dynamics in the absence of activity, $\alpha = 0$, an example of which is shown in Fig. 5. The initial condition is chosen that a pair of $1/2$ and $-1/2$ defects is well separated. If only alignment effects are present, which are described by terms proportional to λ , then the system relaxes to a uniform state. As seen in Fig. 5, the two defects come closer, until they annihilate (the distance between them becomes smaller than the core size) and the orientation becomes uniform, which is the ground state or equilibrium state. This shows once more that what is going on below the microscopic scale a does not affect the macroscopic behavior of the system. As a result of the merging, translational invariance is restored.

In Fig. 6, we have also plotted the Landau-deGennes free energy Eq. (5) as a function of time, which is seen to decrease monotonically. As a uniform state is reached, the Landau-deGennes free energy approaches a constant value. The relaxation toward the uniform value becomes slower as the alignment parameter decreases.

B. Active dynamics

Next we consider the case where both λ and α are nonzero. Finite activity ($\alpha \neq 0$) pumps energy into the system, so we expect defects to be created. On the other hand, there is competition with the alignment terms, which cause defects to annihilate. This is indeed seen in Fig. 7, where the two defects are seen with their center of mass at the origin. In fact, we can choose any origin, since the Stokes equation is invariant under an arbitrary uniform translation. The initial

condition is marked by green squares. At first the two defects move away from one another, but eventually they turn and come closer to one another, and annihilate, as their distance becomes smaller than the core size. However, a new pair is created immediately and starts to move apart, and the process repeats itself. This corresponds very well to what is observed by Refs. [16,19,20,42], where typically annihilation is followed immediately by creation of a new pair. These dynamics are characterized by a rotational component (governed by $\zeta_{1,2}$) and a radial one (governed by the parameters E_1 and D_1); as they approach one another or move apart, pair of defects trace spiral-like trajectories (shown in Fig. 7). The creation and annihilation of defects will eventually lead to a steady-state density of defects when the creation and annihilation balance out. This implies an average distance between the defect cores, Δ (the inverse of which determines the density of defects). We estimate this distance by considering a pair of defects at varying initial distances from each other and numerically finding the critical initial distance for which they neither approach nor repel each other. At small values of α , we find a scaling law

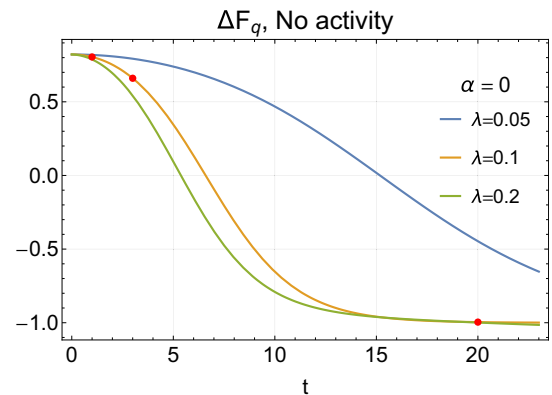


FIG. 6. The evolution of the Landau-deGennes free-energy function as a function of time is plotted for different values of λ . The points indicated on the curve correspond to the three profiles plotted above in Fig. 5.

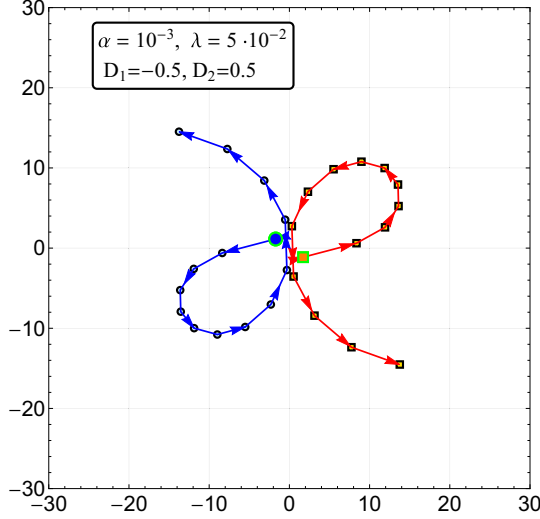


FIG. 7. Trajectory of a pair of defects (in the frame of reference of their center of mass) in the presence of low activity, $\alpha = -10^{-3}$, $\lambda = 10^{-2}$. Circles represent $-1/2$ and squares $+1/2$ defects. As the initial configuration (larger highlighted shapes) evolves, the disclinations trace a spiral, annihilating and then creating a new pair and growing further apart several times.

$\Delta \propto \alpha^{-1/2}$ which has been observed previously numerically in Refs. [26,27].

It is possible to understand the scaling $\alpha^{-1/2}$ by examining the equations for the dynamics of Q_1 , which is the field that governs the distance between the two defects in a pair. Keeping the terms with lowest-order gradients, the equations read

$$\begin{aligned} \eta \nabla^4 \psi &= -2(\alpha + \lambda \Lambda^2 + \lambda \nabla^2) \partial_x \partial_y \delta Q_1 - \alpha (\partial_x^2 - \partial_y^2) \delta Q_2 \\ \partial_t \delta Q_1 &= \lambda (\partial_x \partial_y \psi) + \nabla^2 \delta Q_1 - \Lambda^2 \delta Q_1. \end{aligned}$$

It is evident that the balance among $-\alpha$, $\lambda \nabla^2$, and $\lambda \Lambda^2$ in the first equation sets a length scale Δ , defined by

$$\alpha \sim \lambda \left(\frac{1}{\Delta^2} + \Lambda^2 \right) \sim \lambda \left(\frac{1}{\Delta^2} + \frac{1}{\ell_Q^2} \right). \quad (25)$$

In the regime where $a = 1 \ll \Delta \ll \ell_Q$, this translates into the scaling law

$$\Delta_c \sim \alpha^{-1/2} \sim \ell_\alpha, \quad (26)$$

which accounts for the behavior observed in Fig. 8 for small α . As the active parameter increases, the relative distance between defects becomes comparable to $a = 1$, this scaling approximation breaks down (as the distance Δ plateaus towards $\Delta = a = 1$).

IV. DISCUSSION

We have formulated a theory for the evolution of the macroscopic structure of a (possibly active) nematic liquid crystal built on a first-principles description of its singularities (topological defects). The dynamics are described principally by the motion of the defects contained in a particular state; however, our equations are for the coefficients of an expansion in modes, and the position of the defects follow as a secondary

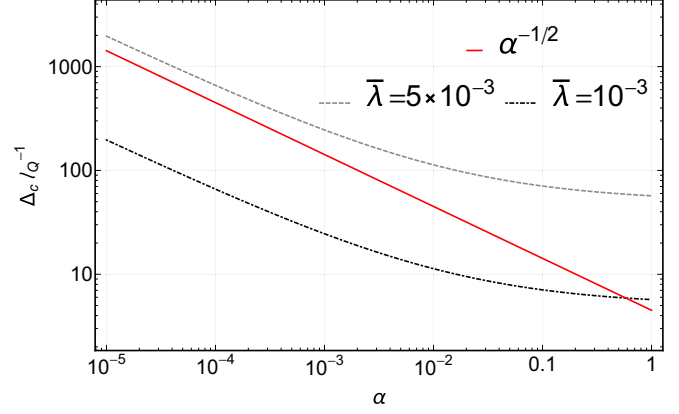


FIG. 8. The average separation between defects plotted as a function of activity. The value of λ is set to 0.1.

quantity. Our simplified dynamics allow for a theoretical prediction of the defect areal density that characterizes the chaotic states observed in Refs. [16,19]. Our result shows a scaling that agrees with that derived by Refs. [26,27] via numerical simulations of the same equations.

In view of experiments and simulations, it would be interesting to describe states with many defects. Although, in principle, by adding more modes in our expansion we can describe states with an arbitrary number of defects, it remains to be seen if this will be practical. An alternative might be to construct superpositions of states made up of *pairs* of equal and oppositely charged defects, which ensures that these states can be matched to each other without encountering any singularities in the fields. For the charge half-disclinations in nematics studied here, our parametrization in terms of \mathbf{Q} rather than \mathbf{n} appears to naturally provide a way for these defects have an orientation and thus makes an important step towards understanding the possibility of defect orientational order as a many-body collective phenomenon [19,43,44].

Most interestingly, the methods we have used can be generalized to analyze groups of topological defects that can be found in a variety of field theories whose dynamics can be described by partial differential equations. Natural examples would be vortices in XY models, polar liquid crystals, or Newtonian fluids. Higher charge defects can also be studied by specifying the appropriate boundary condition at the imposed defect core. Another interesting direction is the study of populations of defects where the vector field lives on a topologically nontrivial manifold such as a sphere [45].

ACKNOWLEDGMENTS

We are grateful to Y. Ibrahim and V. Slastikov for helpful discussions. T.B.L. acknowledges support of BrisSynBio, a Biotechnology and Biological Sciences Research Council (BBSRC)/Engineering and Physical Sciences Research Council (EPSRC) Advanced Synthetic Biology Research Centre (Grant No. BB/L01386X/1).

APPENDIX A: $\mathbf{Q}(\mathbf{r})$ INSIDE THE CORE

The explicit solution for the Q tensor inside the core (for $r < a$) for an imposed defect whose center is at the origin is

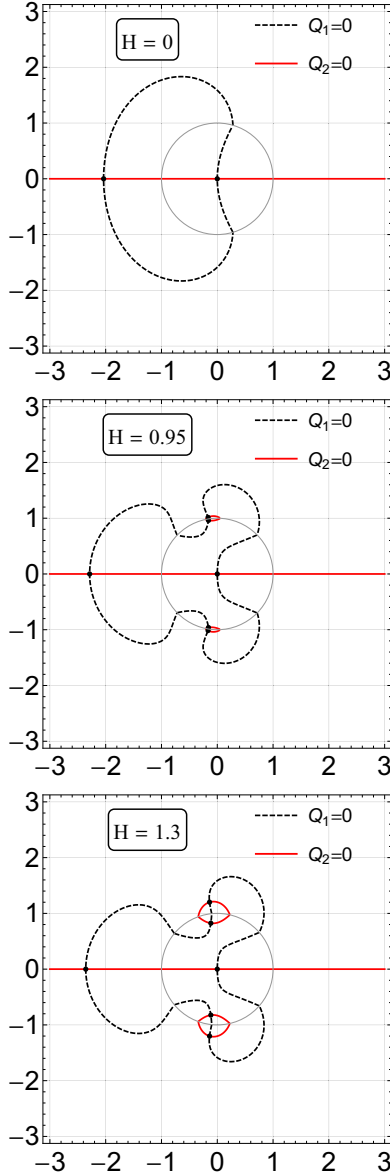


FIG. 9. Level lines $Q_{1,2} = 0$ (dashed black and solid red, respectively) for a solution with three modes. The gray line indicates the core boundary $r = 1$. The intersection points (black dots) represent the positions of the topological defects. As the magnitude of the third mode H increases, the level lines change shape and new pairs of defects appear. In the central panel two extra pairs are produced at the interface $r = 1$; on the right we see that by varying H the positions of different pairs and of the single disclinations within pairs changes. Here $G_{1,2} = 0.1, E_{1,2} = 0, D_{1,2} = 0.9, \zeta_{1,2} = 0$ and $H_{1,2} = H$ in Eqs. (B1) and (B2).

given by

$$Q_1^<(r, \phi) = \frac{E_1}{2} f_1(r, \phi) + \frac{D_1}{2} \frac{J_1(\Lambda r)}{J_1(\Lambda)} \cos(\phi + \zeta), \quad (\text{A1})$$

$$Q_2^<(r, \phi) = q D_2 r \sin(\phi + \zeta) + \frac{E_2}{2} f_2^<(r, \phi), \quad (\text{A2})$$

where

$$f_1(r, \phi) = \sum_{n=1}^{\infty} \frac{\sin \frac{n\pi}{2}}{\pi n} \cos\left(\frac{n}{2}\phi\right) \frac{J_{n/2}(\kappa r)}{J_{n/2}(\kappa a)}$$

and

$$f_2^<(r, \phi) = \frac{4}{\pi} \left[\cot^{-1} \left(\frac{\sec \frac{\phi}{2}}{r^{1/2}} - \tan \frac{\phi}{2} \right) + \cot^{-1} \left(\frac{\sec \frac{\phi}{2}}{r^{1/2}} + \tan \frac{\phi}{2} \right) \right].$$

These solutions have the property that both Q_1, Q_2 vanish at the defect center as expected.

APPENDIX B: GENERATING MORE DEFECTS

While the discussion in the manuscript has mainly considered a single nonzero, i.e., $n = 1$, mode only, the analysis can be extended to higher modes. As an example, in Fig. 9 we show the evolution of solutions that have three allowed modes $n = 1, 2$, and 3:

$$\begin{aligned} \delta Q_1 = & (E_1 - 1) \frac{K_0(\Lambda r)}{K_0(\Lambda)} + D_1 \frac{K_1(\Lambda r)}{K_1(\Lambda)} \cos(\phi + \zeta_1) \\ & + G_1 \frac{K_2(\Lambda r)}{K_2(\Lambda)} \cos(2\phi + \zeta_1) + H_1 \frac{K_3(\Lambda r)}{K_3(\Lambda)} \\ & \times \cos(3\phi + \zeta_1), \end{aligned} \quad (\text{B1})$$

$$\begin{aligned} \delta Q_2 = & E_2 f_2(r, \phi) + D_2 \frac{\sin(\phi + \zeta_2)}{r} + G_2 \frac{\sin(2\phi + \zeta_2)}{r^2} \\ & + H_2 \frac{\sin(3\phi + \zeta_2)}{r^3}. \end{aligned} \quad (\text{B2})$$

Starting with two defects (amplitudes of modes $n = 2, 3$ set to zero), it shows the bifurcations leading to the production of two more pairs of defects. Our analysis indicates that n defect pairs can be created with n modes.

- [1] N. D. Mermin, *Rev. Mod. Phys.* **51**, 591 (1979).
- [2] J. W. Milnor, *Topology from the Differentiable Viewpoint* (Princeton University Press, Princeton, NJ, 1997).
- [3] P. G. D. Gennes and J. Prost, *The Physics of Liquid Crystals* (Clarendon Press, Oxford, 1993).
- [4] K. H. M. Yokota, Y. Hisakado, H. Yang, and T. Kajiyama, *Nat. Mater.* **1**, 64 (2002).
- [5] I. Freund, *Opt. Commun.* **181**, 19 (2000).
- [6] A. V. Ilyenkov, L. V. Kreminskaya, M. S. Soskin, and M. V. Vasnetsov, *J. Nonlin. Opt. Phys. Mater.* **181**, 19 (2000).
- [7] M. V. Berry and M. R. Dennis, *J. Phys. A: Math. Theor.* **40**, 65 (2007).
- [8] T. B. Saw, A. Doostmohammadi, V. Nier, L. Kocgozlu, S. Thampi, Y. Toyama, P. Marcq, C. T. Lim, J. M. Yeomans, and B. Ladoux, *Nature* **544**, 212 (2017).

- [9] K. Kawaguchi, R. Kageyama, and M. Sano, *Nature* **545**, 327 (2017).
- [10] J. E. Moore, *Nature* **464**, 194 (2010).
- [11] X.-G. Wen, *Rev. Mod. Phys.* **89**, 041004 (2017).
- [12] J. Eggers and M. A. Fontelos, *Singularities: Formation, Structure, and Propagation* (Cambridge University Press, Cambridge, 2015).
- [13] P. G. Saffman, *Vortex Dynamics* (Cambridge University Press, Cambridge, 1992).
- [14] F. Bethuel, H. Brezis, and F. Hélein, *Ginzburg-Landau Vortices* (Birkhäuser, Boston, 1994).
- [15] M. C. Marchetti, J. F. Joanny, S. Ramaswamy, T. B. Liverpool, J. Prost, M. Rao, and R. A. Simha, *Rev. Mod. Phys.* **85**, 1143 (2013).
- [16] T. Sanchez, D. T. N. Chen, S. J. DeCamp, M. Heymann, and Z. Dogic, *Nature* **491**, 431 (2012).
- [17] Y. Sumino, K. H. Nagai, Y. Shitaka, D. Tanaka, K. Yoshikawa, H. Chaté, and K. Oiwa, *Nature* **483**, 448 (2012).
- [18] V. Schaller and A. R. Bausch, *Proc. Natl. Acad. Sci. USA* **110**, 4488 (2013).
- [19] S. J. DeCamp, G. S. Redner, A. Baskaran, M. F. Hagan, and Z. Dogic, *Nat. Mater.* **14**, 1110 (2015).
- [20] P. Guillamat, J. Ignés-Mullol, and F. Sagués, *Nat. Commun.* **8**, 564 (2017).
- [21] J. Kosterlitz and D. Thouless, *J. Phys. C: Solid State Phys.* **6**, 1181 (1973).
- [22] F. C. Frank, *Discuss. Faraday Soc.* **25**, 19 (1958).
- [23] L. Giomi, L. Mahadevan, B. Chakraborty, and M. F. Hagan, *Nonlinearity* **25**, 2245 (2012).
- [24] S. P. Thampi, R. Golestanian, and J. M. Yeomans, *Phys. Rev. Lett.* **111**, 118101 (2013).
- [25] H. H. Wensink, J. Dunkel, S. Heidenreich, K. Drescher, R. E. Goldstein, H. Löwen, and J. M. Yeomans, *Proc. Natl. Acad. Sci. USA* **109**, 14308 (2012).
- [26] L. Giomi, *Phys. Rev. X* **5**, 031003 (2015).
- [27] E. J. Hemingway, P. Mishra, M. C. Marchetti, and S. M. Fielding, *Soft Matter* **12**, 7943 (2016).
- [28] L. M. Pismen, *Phys. Rev. E* **88**, 050502(R) (2013).
- [29] L. Giomi, M. J. Bowick, P. Mishra, R. Sknepnek, and M. C. Marchetti, *Philos. Trans. Roy. Soc. A* **372**, 20130365 (2014).
- [30] X.-q. Shi and Y.-q. Ma, *Nat. Commun.* **4**, 3013 (2013).
- [31] H. Pleiner, *Phys. Rev. A* **37**, 3986 (1988).
- [32] G. Ryskin and M. Kremenetsky, *Phys. Rev. Lett.* **67**, 1574 (1991).
- [33] C. W. Oseen, *Trans. Faraday Soc.* **29**, 883 (1933).
- [34] A. Sonnet, A. Kilian, and S. Hess, *Phys. Rev. E* **52**, 718 (1995).
- [35] P. M. Chaikin and T. C. Lubensky, *Principles of Condensed Matter Physics* (Cambridge University Press, Cambridge, 1995).
- [36] A. M. Luo, L. M. Sagis, and P. Ilg, *J. Chem. Phys.* **140**, 124901 (2014).
- [37] E. Lauga and H. A. Stone, *J. Fluid Mech.* **489**, 55 (2003).
- [38] I. S. Gradshteyn and I. M. Ryzhik, *Table of Integrals Series and Products* (Academic Press, New York, 2014).
- [39] S. A. Edwards and J. M. Yeomans, *Europhys. Lett.* **85**, 18008 (2009).
- [40] L. D. Landau and E. M. Lifshitz, *Fluid Mechanics* (Pergamon Press, Oxford, 1984).
- [41] J. Happel and H. Brenner, *Low Reynolds Number Hydrodynamics* (Martinus Nijhoff, The Hague, 1983).
- [42] K.-T. Wu, J. B. Hishamunda, D. T. N. Chen, S. J. DeCamp, Y.-W. Chang, A. Fernández-Nieves, S. Fraden, and Z. Dogic, *Science* **355**, 1284 (2017).
- [43] A. J. Vromans and L. Giomi, *Soft Matter* **12**, 6490 (2016).
- [44] X. Tang and J. V. Selinger, *Soft Matter* **13**, 5481 (2017).
- [45] F. C. Keber, E. Loiseau, T. Sanchez, S. J. DeCamp, L. Giomi, M. J. Bowick, M. C. Marchetti, Z. Dogic, and A. R. Bausch, *Science* **345**, 1135 (2014).